JOURNAL OF MATERIALS SCIENCE 31 (1996) 551–557

Structure and phase transformation of lanthanum chromate

J. D. CARTER*§, H. U. ANDERSON*, M. G. SHUMSKY
*Department of Ceramic Engineering and Graduate Center for Materials Research, University of Missouri-Rolla, Rolla, MI 65401, USA

Lanthanum chromate ($LaCrO_4$) was synthesized as a low temperature ($< 700\,^{\circ}C$) intermediate to perovskite-type, lanthanum chromite ($LaCrO_3$). The lattice parameters, atom positions and bond lengths determined from X-ray powder diffraction show that $LaCrO_4$ forms a monazite-type crystal structure. Lanthanum chromate forms a solid solution with Ca, having a solubility between 10 and 20 at%. Thermal analysis shows that at ambient oxygen pressure, $LaCrO_4$ transforms to $LaCrO_3$ at a temperature near 700 °C. It also indicates that $(La,Ca)CrO_4$ initially transforms to $LaCrO_3$ and $CaCrO_4$ with the subsequent formation of a $(La,Ca)CrO_3$ solid solution. Evidence of Ca segregation to the surface of $(La,Ca)\,CrO_3$ particles is given by Auger electron spectroscopy and scanning electron microscopy.

1. Introduction

Calcium-doped lanthanum chromite $(La,Ca)CrO_3$ has been considered as an interconnect material for the solid oxide fuel cell. It has an electrical conductivity at 1000 °C ranging from 1 to 60 $S\,cm^{-1}$ in a oxygen partial pressure range of 1.013×10^{-15} to 1.013×10^5 Pa [1], respectively; and its thermal expansion coefficient can be matched with yttria-stabilized zirconia [2].

In addition to regulating the electrical conductivity and the thermal expansion coefficient, at temperatures within the two phase region ($700\,^{\circ}C < T < 1000\,^{\circ}C$), Ca exsolves from $(La,Ca)CrO_3$ with Cr to form low temperature melting compounds from the Ca–Cr–O phase system. These are hereafter referred to as $Ca_m(CrO_4)_n$ (following the notation of Sakai *et al.* [3]). These compounds melt at temperatures as low as 1030 °C and are useful for liquid phase sintering. Studies of these compounds indicate that their compositions depend on the A/B ratio (referring to ABO_3) in $(La,Ca)CrO_3$ [4], [5].

A necessary condition when using the $Ca_m(CrO_4)_n$ liquid for sintering is that after the densification process, it should dissolve into the $(La,Ca)CrO_3$ matrix yielding a single phase solid solution. A previous study [6] has shown that the ability to form a solid solution depends on both the solubility of Ca in $(La,Ca)CrO_3$ as well as the distribution of the liquid phase in the system. If either the volume of the liquid phase is too large, or if it is non-uniformly distributed, the kinetics of dissolution and the solubility limits make it difficult to form a single phase. Consequently, the quantity and uniformity of the exsolved liquid phase must be controlled throughout all the processing steps of $(La,Ca)CrO_3$.

Ideally, one would like to work with a powder in which the transient liquid phase exsolves only during the sintering process and then dissolves into the matrix after densification is complete. Thus for liquid phase sintering, it is desirable to prepare $(La,Ca)CrO_3$ powder which has a homogeneous distribution of phases.

This report summarizes the synthesis and characterization of the crystal structure of pure and Ca-doped $LaCrO_4$. In addition, the Ca solubility is determined and a description is given of the transformation of $LaCrO_4$ to $LaCrO_3$, as well as the segregation and distribution of $CaCrO_4$ in $(La,Ca)CrO_3$.

2. Experimental procedure

Powders were synthesized as the compositions $LaCrO_4$ and $La_{0.99-x}Ca_xCrO_4$ where $x = 0.1$, 0.2, 0.3, 0.4. The latter were prepared with an A site deficiency to avoid the formation of unstable Ca excess phases. The notation, $La_{0.99-x}Ca_xCrO_4$ refers to as-synthesized compositions. Although the formula indicates a non-stoichiometric composition with respect to the A/B ratio, it is assumed that solid solutions of calcium-doped $LaCrO_4$ in thermodynamic equilibrium are largely stoichiometric with respect to this ratio (i.e. A/B = 1). Non-stoichiometry within the system is assumed to be manifested in the formation of a second phase. When referring to a stoichiometric solid solution the general notation, $(La,Ca)CrO_4$ is used.

The low temperature liquid mix process [7] was used to synthesize $LaCrO_4$ and $La_{0.99-x}Ca_xCrO_4$. Appropriate amounts of $La_2(CO_3)_3$ and $CaCO_3$

§*Present address*: Chemical Technology Division, Argonne National Laboratory, 9700 South Cass Ave., Argonne, Illinois 60439-4837, USA.

having a nominal purity of 99 at %, were dissolved into a $Cr(NO_3)_3$ solution with the addition of 1 ml deionized water and 0.2 ml nitric acid per gram of dry carbonate. The mixture was heated to ~ 80 °C to dissolve the solids. A 1:1 molar mixture of ethylene glycol (EG) and citric acid (CA) was added to the solution so that the molar ratio of $EG:CA:La_{0.99-x}Ca_xCrO_4 = 1:1:1$. The solution was then heated to its boiling point (about 90 °C), evolving water and nitrogen oxides. The resulting viscous solution was poured into a preheated ceramic dish in a drying oven at 120 °C. The solution boiled rapidly, producing a foam and then charred. This amorphous char was milled in reagent ethyl alcohol for 8 h to yield a powder from the char residue.

Lanthanum chromate was formed by heating the milled char at a rate of 100 °C h^{-1} to 550 °C and holding for 8 h in a flowing argon atmosphere. The argon atmosphere reduced the rate of organic burnoff, thus avoiding the possibility of raising the internal temperatures of the powder above the $LaCrO_4$ to $LaCrO_3$ transformation temperature.

The crystallographic data for $LaCrO_4$ and $(La,Ca)CrO_4$ were obtained from X-ray powder diffraction (XRD; Model 2000, Scintag Inc.) Specimens were analysed at room temperature using Ni-filtered $CuK\alpha_1$ radiation, $\lambda = 0.154$ nm. Silicon powder was used as an internal standard. Measurements were collected over the range of 15–60° 2θ, at 0.03° 2 θ intervals, with a 1 s scan time.

The diffraction pattern corresponded to published data of Manca and Baran [8]. Using their structural model, the lattice parameters were determined by fitting the XRD pattern to the monoclinic system [9, 10]. The model was then refined using a Rietveld analysis program [11]. Initial estimates of the atom positions were taken from $CePO_4$ data [12]. The XRD data used for Rietveld refinement were collected over the range of 15–100° 2θ at 0.03° 2θ intervals with a 4 s scan time.

Phase transformations were studied using simultaneous differential thermal analysis and thermogravimetric analysis (DTA/TGA; Model 409, Netzsch Inc.) at heating rates of 1 and 10 °C min^{-1} to peak temperatures of 1400 °C. Platinum crucibles were used to minimize possible reactions with the powder.

Phase segregation was observed by scanning electron microscopy (SEM; Jeol model T33A). Surface analysis was performed using auger electron spectroscopy (AES; Perkin Elmer model 545) on compacted powders of $La_{0.99-x}Ca_xCrO_3$ where $x = 0.1$ and 0.3. The perovskite phase was obtained by calcining char powders at 800 °C for 8 h. Specimens were uniaxially pressed at 70 MPa to form a 1.2 cm disc. Specimens sintered at 1400 °C for 2 h were also analysed by AES.

TABLE I X-ray powder diffraction data for $LaCrO_4$

d_{obs} (nm)	d_{calc} (nm)	I/Io_{obs}	*hkl*
0.5437	0.5439	10	$10\bar{1}$
0.4955	0.4957	7	110
0.4818	0.4822	7	$01\bar{1}/011$
0.4346	0.4348	17	$11\bar{1}$
0.4180	0.4180	6	101
0.3617	0.3619/0.3618	16	111/*020
0.3399	0.3401	62	200
0.3233	0.3234	4	002
0.3194	0.3195	100	120
0.3156	0.3158	< 1	$02\bar{1}/021$
0.3077	0.3078/0.3071	16	$*210/21\bar{1}$
0.2974	0.2976	23	$11\bar{2}$
0.2952	0.2952	30	$01\bar{2}/012$
0.2719	0.2720	19	$20\bar{2}$
0.2546	0.2558/0.2546	19	$211/*21\bar{2}$
0.2501	0.2502	10	112
0.2477	0.2478/0.2475	5	$*220/22\bar{1}$
0.2423	0.2424	3	$12\bar{2}$
0.2335	0.2336	3	$30\bar{1}$
0.2273	0.2274	1	130
0.2260	0.2260	7	$03\bar{1}/031$
0.2225	0.2227/0.2223	13	$103/31\bar{1}$
0.2182	0.2181	10	221
0.2165	0.2174/0.2164	2	$22\bar{2}/310$
0.2090	0.2089	2	131
0.2046	0.2046	3	$31\bar{2}$
0.2007	0.2008	32	212
0.1985	0.1986	3	301
0.1967	0.1966	7	$23\bar{1}$
0.1940	0.1940	30	$13\bar{2}$
0.1920	0.1921/0.1918/0.1915	15	*320/103/311
0.1852	0.1852	3	$023/023$
0.1837	0.1837	19	$32\bar{2}$
0.1808	0.1813/0.1809/0.1809	5	$30\bar{3}$/*040/231
	0.1805/0.1803		$/23\bar{2}/22\bar{3}$
0.1789	0.1789	23	132
0.1748	0.1748	12	140
0.1710	0.1710	1	$41\bar{1}$
0.1696	0.1701/0.1696	9	$400/*40\bar{2}$
0.1655	0.1656/0.1652/0.1651	6	$*410/330/41\bar{2}$

*These peaks have significantly greater intensities than others in the series.

3. Results and discussion

3.1. $LaCrO_4$ formation

A previous study [13] suggested that perovskite $LaCrO_3$ formed directly from the char when the temperature exceeded 500 °C. However, a preliminary investigation in this study showed that a mixture of $LaCrO_4$ and $LaCrO_3$ often formed at calcination temperatures below 600 °C.

Since it is well known that heat from oxidation of the organic during the liquid mix process raises the internal temperature of the powder several hundred degrees above the furnace temperature, it is likely that the combustion of the organics provided enough heat for partial, if not complete transformation of $LaCrO_4$ to $LaCrO_3$, which occurs in the 650 to 700 °C range.

It was found that the circulation of argon in the furnace during calcination greatly reduced the combustion rate of the organics, thereby allowing the actual internal powder temperature to remain below the $LaCrO_4$ to $LaCrO_3$ transformation temperature.

3.2. Crystallographic data

Table I is a summary of the *d*-spacings, relative intensities (I/Io_{obs}) and *hkl* indexing. The observed *d*-spacing (d_{obs}) values generally agree with those reported by Manca and Baran [8]. They concluded that $LaCrO_4$

TABLE II Crystal data for monoclinic $LaCrO_4$

Space group	$P2_1/n(C_{2h}^5)$
a (nm)	0.7041(1)
b (nm)	0.7237(1)
c (nm)	0.6693(1)
β	104.94°
V $(nm)^3$	0.3295
Z	4
Dx $(g\,cm^3)$	5.138

crystallizes in a monazite-type structure ($CePO_4$), which belongs to the $P2_1/n\,(C_{2h}^5)$ space group.

The present study identified some additional peaks in the diffraction pattern which were not previously recorded. These extra peaks lie in the relative intensity range from 1 to 10%. The calculated d-spacings (d_{calc}) were determined from the lattice parameters given in Table II.

The results of Rietvelt refinement are plotted in Fig. 1. The measured data are indicated by points and the refined model is indicated by lines. The narrow plot below the main diagram shows intensity differences between measured and calculated values.

Agreement between the model and observed data can be quantified by the profile (R_p) and weighted profile (R_{WP}) values given by the formulae [14]

$$R_P = \frac{\Sigma |y_{io} - y_{ic}|}{\Sigma y_{io}} \quad (1)$$

$$R_{WP} = \left[\frac{\Sigma w_i (y_{io} - y_{ic})^2}{\Sigma w_i y_{io}^2}\right]^{1/2}$$

where y_{io} is the observed intensity at the ith step, y_{ic} is the intensity calculated from the structural model, and w_i is a weight factor given by $(w_i)^{-1} = \sigma_{ip}^2 + \sigma_{ib}^2$. This sum is based on standard deviations associated with the counting statistics of a given peak (σ_{ip}^2) and with the background intensity (σ_{ib}^2).

In the present investigation, the values determined from the refined data of $LaCrO_4$ are $R_P = 0.071$ and $R_{WP} = 0.098$.

Table III lists the refined fractional co-ordinates and temperature factors, B (nm^3) of the atoms in the $LaCrO_4$ crystal structure. In this structure, lanthanum is surrounded by nine O atoms; the distances of La–O are 0.119, 0.183, 0.242, 0.242, 0.248, 0.255, 0.264, 0.274 and 0.282 ± 0.001 nm. Chromium is in a distorted tetrahedral site surrounded by four O atoms. The distances of Cr–O are 0.164, 0.168, 0.170 and 0.172 ± 0.001 nm. These results agree with a description of the monazite structure in the literature [12].

3.3. Calcium solubility

X-ray diffraction studies on $La_{0.99-x}Ca_xCrO_4$ indicate a solubility limit of $0.1 \leqslant x \leqslant 0.2$. This is approximately the same solubility as in $LaCrO_3$ [6]. Fig. 2 is a plot of the unit cell volume of monazite-type $(La,Ca)CrO_4$ versus Ca content. The volume initially decreases with increasing Ca, which is an indication

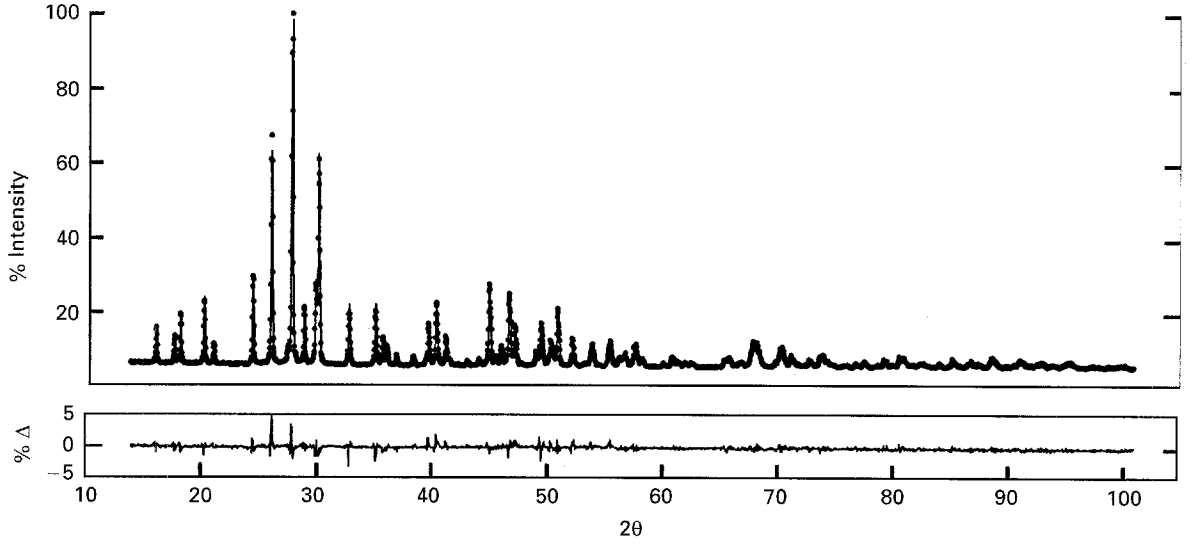

Figure 1 Top: A comparison of $LaCrO_4$ X-ray powder diffraction data with the $P2_1/n$ structural model. Bottom: Intensity difference between the data and the model. —— model; ● data.

TABLE III Refined fractional co-ordinates for the atoms in monoclinic $LaCrO_4$

	La	Cr	OI	OII	OIII	OIV
x	0.221(1)	0.198(1)	0.258(2)	0.024(2)	0.373(2)	0.115(2)
y	0.157(1)	0.165(1)	0.002(2)	0.110(2)	0.212(2)	0.336(2)
z	0.397(1)	0.886(1)	0.079(2)	0.680(2)	0.760(2)	0.011(2)
B(nm^2)[a]	0.0029(4)	0.0058(7)	0.0056	0.0064	0.0062	0.0069

[a]B, atomic temperature factor.

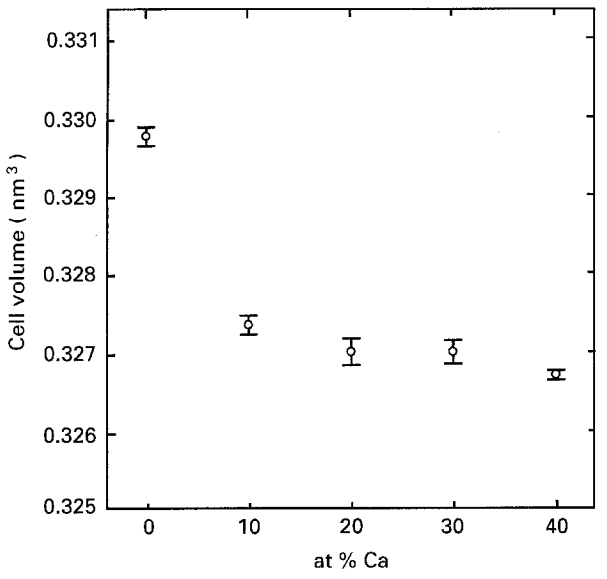

Figure 2 Unit cell volume versus Ca content of $LaCrO_4$ and $La_{0.99-x}Ca_xCrO_4$ solid solutions, where $0.1 \leqslant x \leqslant 0.4$.

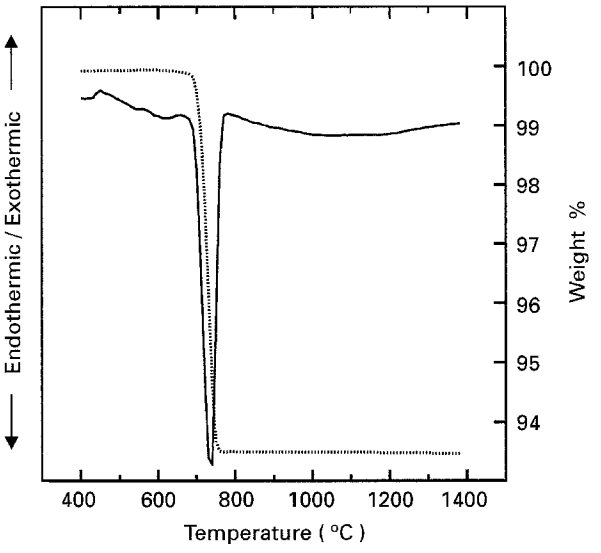

Figure 3 Combined DTA (—)/TGA (. . . .) data for $LaCrO_4$. Heating rate, 1 °C min^{-1}

that the smaller Ca ion is replacing La in the structure. However, from 20 to 40 at % Ca, the cell volume is relatively constant. This suggests that Ca has reached its solubility limit. A detailed XRD study revealed the appearance of $CaCrO_4$ peaks in the 30 and 40 at % Ca compositions.

Calcium chromate crystallizes in a zircon-type structure, which belongs to the $I4_1/amd$ (D_{4h}^{19}) space group [15]. According to Wyckoff [16], the structure is composed of linked $Ca^{II}O_4$ and $Cr^{VI}O_4$ tetrahedra. In contrast, the monazite-type $LaCrO_4$ structure has distorted $Cr^{V}O_4$ tetrahedra and La^{III} atoms co-ordinated by nine oxygens. Transformation between the two structures must be reconstructive, since Ca atoms would change from a 4-fold in the zircon-type structure, to a 9-fold co-ordination in the monazite-type structure in forming a solid solution with $LaCrO_4$. In view of this, it is reasonable that $CaCrO_4$ would show a solubility limit in $LaCrO_4$. This is evident from the present results.

3.4. $LaCrO_4$ phase transformation

X-ray analysis showed that at temperatures above 700 °C, the monazite-type structure becomes unstable and transforms to perovskite-type $LaCrO_3$. This necessarily involves the release of oxygen according to the reaction

$$LaCrO_4 \rightarrow LaCrO_3 + \tfrac{1}{2}O_2 \qquad (2)$$

The transformation between the two crystal structures is complex and not well understood, but a comparison of the monazite to the perovskite structure [17] shows that La atoms change from a 9-fold to a 12-fold oxygen co-ordination and Cr atoms change from a tetrahedral to an octahedral O coordination. According to electrical neutrality conditions, the Cr atoms are reduced from a +5 to +3 valence, and one O atom per formula unit diffuses out of the bulk crystal to a free surface and is released into the atmosphere. These crystallographic changes cause a unit cell volume decrease from 0.33 to 0.23 nm^3.

The $LaCrO_4$ to $LaCrO_3$ transformation was readily observed with DTA and TGA. The DTA/TGA data in Fig. 3 shows the $LaCrO_4$ to $LaCrO_3$ transformation occurring at 680 ± 10 °C. The TGA curve yields a weight loss of 6.4 ± 0.1 wt % which agrees with the loss of oxygen (6.3 wt %) predicted by Equation 2. No other interactions or weight changes occurred as the temperature increased to 1400 °C.

When Ca is added to $LaCrO_4$, the DTA/TGA and XRD results change. The 10 at % Ca composition is single phase in the monazite-type structure and in the perovskite-type structure at temperatures above 800 °C. Since the 10% composition is single phase, it is not interesting in the context of low temperature sintering, so the DTA/TGA study concentrated only on compositions with 20 at % or higher Ca content. For Ca content > 10 at %, thermal analyses showed two endothermic reactions between 600 and 1100 °C, each accompanied with a weight loss.

Figs 4 and 5 illustrate the DTA/TGA analysis of $CaCrO_4$ and $La_{0.99-x}Ca_xCrO_4$ with $x = 0.2$, 0.3 and 0.4. The first reaction between 600 and 700 °C is related to the transformation of $LaCrO_4$ to $LaCrO_3$. The transformation temperature shows no systematic behaviour with respect to Ca content. However, TGA behaviour shows decreasing weight loss values at the transformation with increasing Ca content.

X-ray analysis on powders calcined at 800 °C indicated the formation of a solid solution of Ca in $LaCrO_3$. Referring to Equation 2 the overall transformation reaction may be written

$$La_{1-u}Ca_uCrO_4 \rightarrow \tfrac{1-u}{1-v}La_{1-v}Ca_vCrO_3 + \tfrac{u-v}{1-v}CaCrO_4 + \tfrac{1-u}{2(1-v)}O_2 \qquad (3)$$

where $u = 0.2$, 0.3, 0.4 and v can be considered as a measure of the initial solubility of Ca in $LaCrO_3$.

Since oxygen is the only species involved in the weight change, the TGA data may be used to calculate

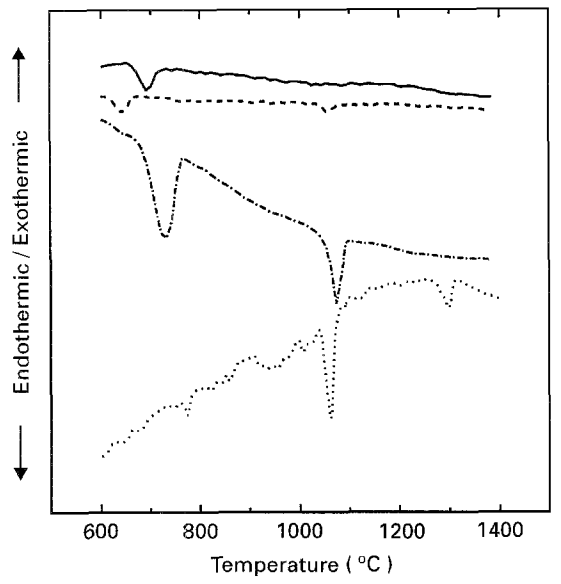

Figure 4 DTA results of $CaCrO_4$ and 20, 30 and 40 at % doped lanthanum chromates. Heating rate, 1 °C min^{-1}—$La_{0.79}Ca_{0.2}CrO_4$; – – – $La_{0.69}Ca_{0.3}CrO_4$; –.–. $La_{0.59}Ca_{0.4}CrO_4$; ----- $CaCrO_4$.

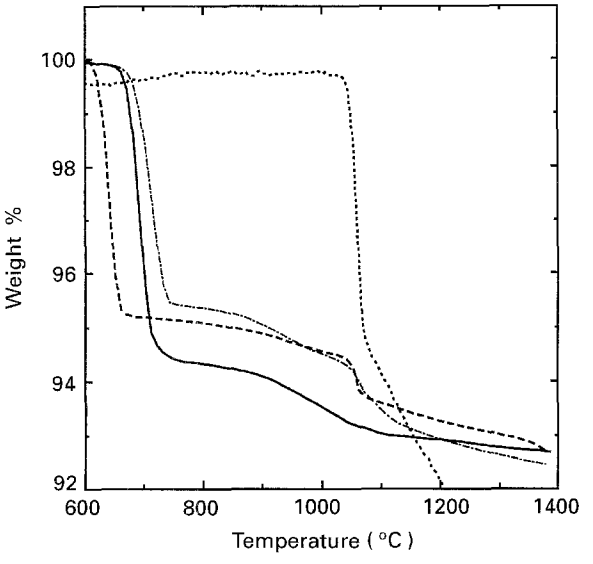

Figure 5 TGA results of $CaCrO_4$ and 20, 30, and 40 at % doped lanthanum chromates. Heating rate, 1 °C min^{-1}—$La_{0.79}Ca_{0.2}CrO_4$; – – – $La_{0.69}Ca_{0.3}CrO_4$; –.–. $La_{0.59}Ca_{0.4}CrO_4$; ----- $CaCrO_4$.

v or the solubility of Ca after the transformation. The solubility is calculated by substituting the corresponding values of u and the oxygen loss into the fraction preceding O_2 in Equation 3 and solving for v. Table IV lists the weight loss and v for 20, 30 and 40 at % Ca additions. Within the experimental error of $\pm$ 1 at %, the values of v are considered to be zero, which suggests that the amount of dissolved Ca after the transition is negligible. Thus the TGA results imply the $(La,Ca)CrO_4$ transforms to $LaCrO_3$ and $CaCrO_4$ and that Ca does not initially form a solid solution with $LaCrO_3$.

As the powders are heated to temperatures beyond the transformation temperature, $CaCrO_4$ loses oxygen and dissolves into $LaCrO_3$ to form a solid solution. This is evident by the weight loss after the transformation (Fig. 5).

TABLE IV Solubility, v, of Ca in $LaCrO_3$ at the phase transformation (600–680 °C), as calculated from thermogravimetric measurements

at % Ca	$\Delta w/w_o$(%)	v
20	5.5 ± 0.1	0.00 ± 0.01
30	4.8 ± 0.1	− 0.04 ± 0.01
40	4.5 ± 0.1	0.00 ± 0.01

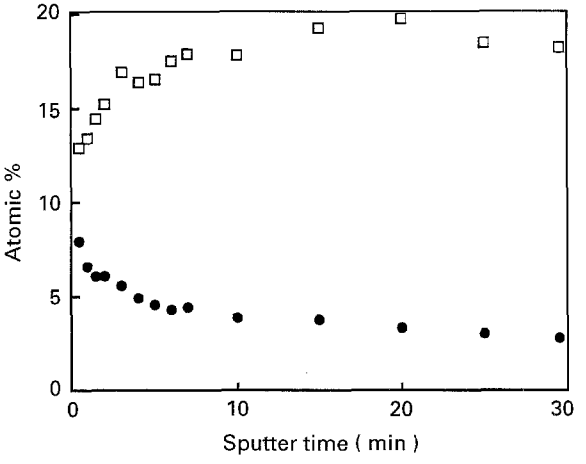

Figure 6 An AES depth analysis of a compact of $La_{0.89}Ca_{0.1}CrO_3$ powder. Calcined at 800 °C for 8 h. □ La; ● Ca.

Near 1030 °C, another endothermic reaction accompanied with an increased rate of weight loss is observed. This corresponds to the melting point of $CaCrO_4$. The melting behaviour of this compound and compositions related to the Ca–Cr–O pseudobinary system has been well characterized [18, 19, 20]. The $La_{0.79}Ca_{0.2}CrO_3$ composition shows no indication of a reaction, presumably since most of the $CaCrO_4$ has dissolved into the $(La,Ca)CrO_3$ matrix before the melting temperature was obtained.

As heating proceeds above the melting point, Ca, Cr, and O continue to dissolve into the $(La,Ca)CrO_3$ matrix. However, the $Ca_m(CrO_4)_n$ liquid also loses weight as indicated by the $CaCrO_4$ curve in Fig. 5. Consequently, the dissolution of Ca, Cr and O into $LaCrO_3$ can no longer be followed by TGA.

3.5. Calcium chromate distribution

Auger electron spectroscopy (AES) disclosed the formation of a Ca rich surface layer in $(La,Ca)CrO_3$ powder. Figs 6 and 7 show the AES surface profiles of $La_{0.89}Ca_{0.1}CrO_3$ and $La_{0.69}Ca_{0.3}CrO_3$ powders, respectively. These had been calcined at 800 °C for 8 h and pressed into discs. X-ray diffraction showed that the 10 at % Ca composition had formed a single phase, whereas the 30 at % composition had formed a solid solution with excess $CaCrO_4$. Increased segregation is observed as the Ca content is increased.

Fig. 8 is an AES depth analysis of $La_{0.89}Ca_{0.1}CrO_3$ sintered at 1400 °C. The fact that no excess Ca is observed at the surface indicates a high solubility of Ca and little, if no segregation of $CaCrO_4$. Similar results are obtained for the 30 mol % Ca composition.

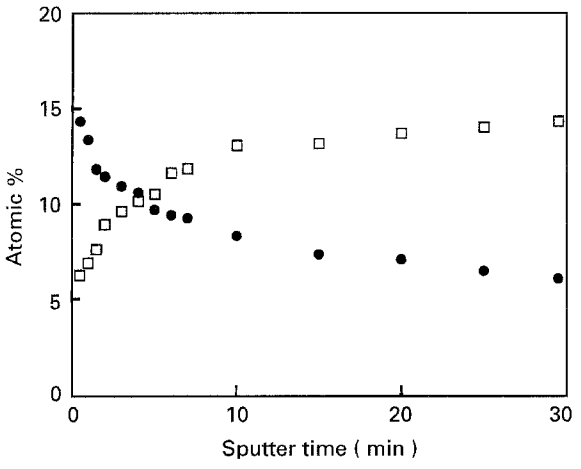

Figure 7 An AES depth analysis of a compact of $La_{0.69}Ca_{0.3}CrO_3$ powder. Calcined at 800 °C for 8 h. □ La; ● Ca.

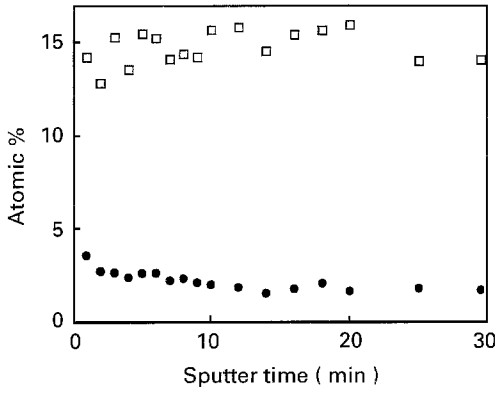

Figure 8 An AES depth analysis of a $La_{0.89}Ca_{0.1}CrO_3$ disc. Sintered at 1400 °C/2 h. □ La; ● Ca.

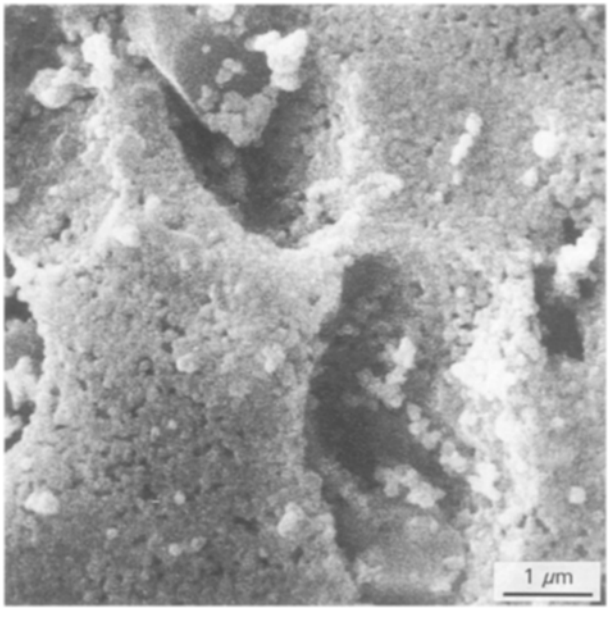

Figure 9 A SEM micrograph of a $La_{0.59}Ca_{0.4}CrO_3$ aggregate showing a segregated $CaCrO_4$ crystal at the top centre. Calcined at 800 °C for 8 h.

X-ray analysis agrees with this, in respect that no $CaCrO_4$ was observed after sintering at 1400 °C.

These observations are related to the solute solubility. When the solubility of Ca in $LaCrO_3$ is low, Ca preferentially segregates to the surface of the primary particle. This becomes evident in AES before it can be detected by XRD. When the solubility of Ca is high, it is stable within the bulk and the surface becomes a homogeneous mixture of La and Ca. A review by Hondros and Seah [21] discusses the theory and phenomenon of surface segregation in detail.

From surface analysis it is concluded that excess Ca will likely segregate to the surface of the $(La,Ca)CrO_3$ particle within temperature ranges of low solubility. It was also observed by SEM that if homogeneous powders with excess $CaCrO_4$ are annealed below 1000 °C for a long enough time, the $CaCrO_4$ will grow on the particle surface and eventually segregate into individual crystals. Such a crystal is evident in the top centre of Fig. 9. If segregation occurs, a non-homogeneous distribution of the $Ca_m(CrO_4)_n$ liquid results. The same distribution of the liquid phase could reduce the effectiveness of sintering or subsequent solid solution formation.

4. Summary

The present investigation has shown that monazite-type $LaCrO_4$ and $(La,Ca)CrO_4$ can be synthesized through the use of the liquid mix process and by calcining in argon at 550 °C. The solubility of Ca in $LaCrO_4$ is between 10 and 20 at %. When $(La,Ca)CrO_4$ was heated to ~ 700 °C, intermediate products, $LaCrO_3$, $CaCrO_4$ and O_2 evolved. The $LaCrO_3$ and $CaCrO_4$ subsequently combined, evolving more O_2, to form a solid solution, $(La,Ca)CrO_3$. For powders heated to 800 °C, Ca was seen to segregate to $(La,Ca)CrO_3$ particle surfaces at low solubility. Scanning electron microscopy showed that crystals of $CaCrO_4$ segregate from the $(La,Ca)CrO_3$ particles. Upon heating to 1400 °C, AES showed that 10 and 30 at % Ca compositions regained a homogeneous mixture of La and Ca at the specimen surface, which was an indication that the solubility of Ca in $(La,Ca)CrO_3$ had increased to form a solid solution.

Acknowledgements

Special thanks is given to Jens Ranløv of Risø National Laboratory for discussions and help with the crystal structure refinement. Financial support was granted in part by Argonne National Laboratories and the division of Basic Energy Science of the US Department of Energy.

References

1. I. YASUDA and T. HIKITA, in Proceedings of the Second International Symposium on Solid Oxide Fuel Cells, Athens, Greece, 1991, edited by F. Gross, P. Zegers, S. C. Singhal, and O. Yamamoto. (Commission of the European Communities, Luxembourg, 1991) p. 645.
2. N. SAKAI, T. KAWADA, H. YOKOKAWA, M. DOKIYA and T. IWATA, *Solid State Ionics* **40/41** (1990) 394.
3. N. SAKAI, T. KAWADA, H. YOKOKAWA, M. DOKIYA and I. KOJIMA, *J. Amer. Ceram. Soc.* **76** (1993) 609.

4. J. D. CARTER, Ph.D. Dissertation, University of Missouri-Rolla, Rolla MO, (1992).
5. L. A. CHICK, T. R. ARMSTRONG, D. E. McCREADY, G. W. COFFEY, G. D. MAUPIN and J. L. BATES, in Proceedings of the Third International Symposium on Solid Oxide Fuel Cells, Honolulu, 1993, Vol. 93-4, edited by S.C. Singhal, and H. Iwahara, (Pennington, NJ, The Electrochemical Society, Inc., 1993) p. 374.
6. J. D. CARTER, V. SPRENKLE, M. M. NASRALLAH, and H. U. ANDERSON, in Proceedings of the Third International Symposium on Solid Oxide Fuel Cells, Honolulu, 1993, Vol. 93-4, edited by S. C. Singhal, and H. Iwahara, (Pennington, NJ, The Electrochemical Society, Inc., 1993) p. 344.
7. L. TAI and P. LESSING, *J. Mater. Res.* **7** (1992) 511.
8. JCPDS Card #36-93, (Joint Committee on Powder Diffraction Standards, Swarthmore, PA, 1986); and S. G. MANCA and E. J. BARAN, *J. Appl. Cryst.* **15** (1982) 102.
9. J. W. VISSER, *Ibid* **2** (1969) 89.
10. MathCAD Ver. 2.5, Mathsoft, Inc. (1989).
11. A. SAKTHIVEL and R. A. YOUNG, in the users guide to DBWS-9006 and DBWS-9006PC programs for Rietveld analysis of X-ray and neutron powder diffraction patterns, (Georgia Institute of Technology, Atlanta, GA, 1992).
12. "Structure Reports" Vol. 17, edited by A. J. C. Wilson, (Oosthoek, Utrecht, Netherlands, 1963) p. 487.
13. H. U. ANDERSON, C. C. CHEN, J. C. WANG and M. J. PENNELL, in "Ceramic transactions Vol. 12, Ceramic powder science III", edited by G. L. Messing, S. Hirano, and H. Hausner (American Ceramic Society, Westerville, OH, 1990) p. 749.
14. C. GIACOVAZZO, in "Fundamentals of crystallography", edited by C. Giacovazzo (Oxford University Press, New York, 1992) p. 109.
15. JCPDS Card #8-458, (Joint Committee on Powder Diffraction Standards, Swarthmore, PA, 1958); and US National Bureau, of Standards Circular 539, **7**, (1957) p. 13.
16. R. W. G. WYCKOFF, "Crystal structures", 2nd edn, Vol. 3 (J Wiley and Sons, New York, 1965) p. 15.
17. C. KHATTAK and D. COX, *Mater. Res. Bull.* **12** (1977) 463.
18. W. F. FORD and J. WHITE, *Trans. Br. Ceram. Soc.* **48** (1949) 417.
19. Z. PÁNEK, *Silikáty* **25** (1981) 169.
20. A. KAISER, B. SOMMER and E. WOERMANN, *J. Amer. Ceram. Soc.* **75** (1992) 1463.
21. E. D. HONDROS and M. P. SEAH, *Int. Metall. Rev.* **22** (1977) 262.

Received 9 February 1994
and accepted 28 April 1995